

# Natural Convection Heat Transfer and Entropy Generation Analysis in Saltbox Roof under Summer Conditions

Tobechukwu E. Ogwumike, \*Olabode T. Olakoyejo, Fisayo T. Oloruntoba, Abdulsohur A. Musah, Manasseh O. Oyekeye, Omotayo Oluwatusin, Adeyinka A. Oluwo, Adekunle O. Adelaja

Department of Mechanical Engineering, University of Lagos, Akoka, Lagos, Nigeria

tobechukwu\_e@yahoo.com | oolakoyejo | moyekeye | ooluwatusin | aoluwo | aadelaja@unilag.edu.ng  
| tobafisayo381 | asmusah12@gmail.com

Received: 30-OCT-2021; Reviewed: 13-DEC-2021; Accepted: 22-APR-2022

<https://doi.org/10.46792/fuoyejet.v7i2.722>

## ORIGINAL RESEARCH ARTICLE

**Abstract-** This study investigates numerically the 2D laminar natural convection in a Saltbox roof type geometry under summer climate conditions as obtained in Africa, particularly Nigeria using ANSYS FLUENT to model the boundary conditions. The effects of Rayleigh number ( $Ra$ ) within the range of  $10^3$ - $10^7$  and pitch angles (top and base) on heat transfer, the flow structure, temperature distribution and entropy generation within the geometry were analysed. Results show that the flow is nearly symmetric at lower  $Ra$ , while for higher  $Ra$ , the flow becomes asymmetric. The Nusselt number ( $Nu$ ) has a proportional relationship with the top pitch angle and an inverse relationship with the base pitch angle when the Rayleigh number is fixed. The effect of the  $Ra$  on the  $Nu$  is insignificant at lower  $Ra$ , but becomes noticeable at higher  $Ra$ . The total entropy generation increases with an increase in top pitch angle and a decrease in base pitch angles, at fixed Rayleigh numbers. The physical implication is that, for a Saltbox roof type geometry, at fixed  $Ra$ , the best convective heat transfer process is achieved by lowering the base pitch angle and increasing the top pitch angle.

**Keywords-** Entropy generation, Natural convection, Nusselt number, Pitch angle, Rayleigh numbers Minimum.

## 1 INTRODUCTION

Natural convection is a vital mode of heat transfer driven by density differences resulting from a temperature gradient. It takes place within the roofing structures and is influenced by the climate condition, either winter or summer climate. Its study helps in improving the energy efficiency of buildings and structures.

Varol et al. (2006) studied the natural convective heat transfer in Saltbox under summer and winter conditions. They observed that lesser heat transfer occurred during summer condition. Solomon and Kamiyo (2020) studied the natural convection heat transfer in a right-angled triangle-shaped rooftop subjected to isothermal heating at the base wall. They observed that the heat transfer rate and pitch angles had an inverse relationship. Increasing the Rayleigh number and pitch angle reduced the number of counter rotating cells. Akinsete and Coleman (1982) studied the 2D laminar convection flow in a right-angled triangular enclosure. They discovered that one-third of the base wall was closer to the intersection of the hypotenuse, and the base was responsible for about 60% of total heat transfer at the base wall. Systems can be optimized by reducing their entropy generation. Alnaqi et al. (2020) studied the natural convection and entropy generation in a cubical cavity and observed that total entropy fairly increased with an increase in Rayleigh number until a certain value, when it then rose significantly.

Similar studies have also been carried out (Bondareva et al., 2017; Hussein et al., 2016; Yang et al., 2021; Zhang et al., 2021; Ishak et al., 2021; Oztop et al., 2017). Natural convection in Saltbox roof is analysed for a hot climate region, with the aim of helping designers improve the thermal comfort in such conditions. Results show that under this condition, at fixed  $Ra$ , the best convective heat transfer process is achieved by lowering the top pitch angle ( $\varphi$ ) and increasing the base pitch angle ( $\alpha$ ).

## 2 MATERIALS AND METHODS

### 2.1 PROBLEM FORMULATION

The physical model of the saltbox roof type geometry currently under study is shown in figure 1. The physical model entails a 3D view of the roofing geometry consisting of roof, ceiling and wall.

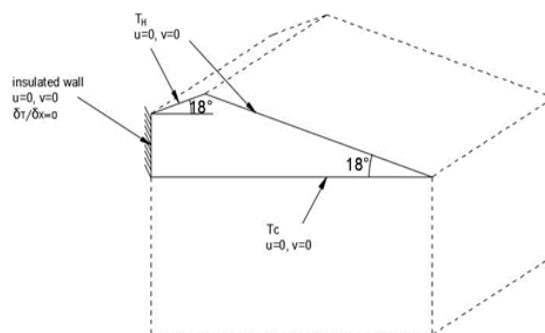


Fig. 1: 3D schematic diagram of saltbox roof type (Koca et al., 2007)

This model is simplified and assumed to be a 2D model. figure 2 shows the computational domain of saltbox roof geometry in natural convective flow. The inclined roof surfaces with top pitch angle ( $\varphi$ ) have a constant hot temperature,  $T_H$ , and the bottom surface (ceiling) with base pitch angle ( $\alpha$ ) has constant cold temperature,  $T_C$ . The vertical wall surface is kept insulated.

\*Corresponding Author

Section C- MECHANICAL/MECHATRONICS ENGINEERING & RELATED SCIENCES

Can be cited as:

Ogwumike T.E., Olakoyejo O.T., Oloruntoba F.T., Musah A.A., Oyekeye M.O., Oluwatusin O., Oluwo A.A. and Adelaja A.O. (2022): Natural Convection Heat Transfer and Entropy Generation Analysis in Saltbox Roof under Summer Conditions, *FUOYE Journal of Engineering and Technology* (FUOYEJET), 7(2), 205-209. <http://doi.org/10.46792/fuoyejet.v7i2.722>

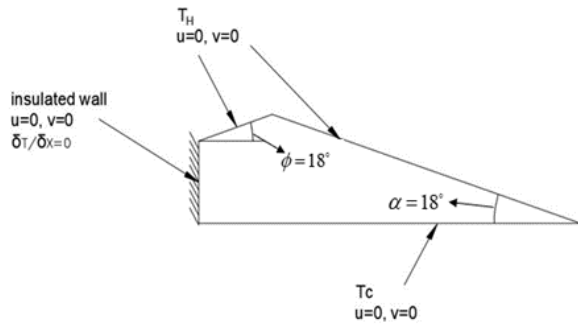


Fig. 2: Computational domain of saltbox roof

This configuration is designed to simulate a hot weather environment as obtainable in West Africa. Thus, the inclined roofs behave as a heater, while the bottom wall (ceiling) is colder than the inclined walls.

**2.2 DESIGN EQUATIONS AND ASSUMPTIONS**

The system is considered a steady state and two-dimensional, having compressible laminar flow regime and Newtonian fluid. The dimensionless forms of governing equations of mass, momentum, and energy are expressed in equations (1) – (4) as:

$$\frac{dU}{dX} + \frac{dV}{dY} = 0 \tag{1}$$

$$\left(\frac{Ra}{Pr}\right)^{\frac{1}{2}} \left( U \frac{dU}{dX} + V \frac{dV}{dY} \right) = -\frac{dP}{dX} + \nabla^2 U \tag{2}$$

$$\left(\frac{Ra}{Pr}\right)^{\frac{1}{2}} \left( U \frac{dU}{dX} + V \frac{dV}{dY} \right) = -\frac{dP}{dY} + \nabla^2 V + \left(\frac{Ra}{Pr}\right)^{\frac{1}{2}} \theta \tag{3}$$

$$(RaPr)^{\frac{1}{2}} \left( U \frac{d\theta}{dX} + V \frac{d\theta}{dY} \right) = \nabla^2 \theta \tag{4}$$

The dimensionless thermal and frictional entropy generation due to irreversibility are expressed in equations (5) and (6) respectively as:

$$S_{thermal} = \left[ \left(\frac{d\theta}{dX}\right)^2 + \left(\frac{d\theta}{dY}\right)^2 \right] \tag{5}$$

$$S_{friction} = \left[ 2 \left[ \left(\frac{dU}{dX}\right)^2 + \left(\frac{dV}{dY}\right)^2 \right] + \left(\frac{\partial U}{\partial Y} + \frac{\partial V}{\partial X}\right)^2 \right] \tag{6}$$

Therefore, total entropy generation is expressed as:

$$S_{Total} = S_{thermal} + S_{friction} \tag{7}$$

The boundary conditions in the dimensionless form are given as:

- i. Wall (roof) bottom  $T_c, U = V = \theta = 0$
- ii. Wall (roof) inclined  $T_H, \theta = 1; U = V = 0$
- iii. Wall symmetry  $U = \frac{dT}{dX} = \frac{dV}{dX} = 0$
- iv. Wall vertical (Insulated),  $q'' = U = V = \frac{dT}{dX} = 0$

**3 NUMERICAL METHOD AND VALIDATION**

ANSYS FLUENT code based on the finite volume method (FVM) and was employed to solve the governing equations and imposed boundary conditions (Patankar & Spalding, 1972). The semi-implicit method for pressure-

linked equations (SIMPLE) scheme algorithm was applied for the pressure-velocity coupling. A second-order upwind scheme was used to discretize the combined convection and diffusion terms in the momentum and energy equations. The solution is believed to have converged when the normalized residuals of the mass and momentum equations fall under  $10^{-10}$  and the residual convergence of the energy equation was less than  $10^{-18}$ . A graphical display of the residual converged solution was shown simultaneously as the simulation was being ran. The results from this simulation were displayed in isotherms and streamlines which showed the temperature distribution across the total surface of the geometry and the total heat transfer rate was gotten for different conditions. A grid dependence test was carried out to certify the accuracy of the result with variation of Nusselt number ( $Nu$ ).  $Nu$  is expressed as in Varol et al. (2006). The convergence criteria are expressed in equation (8). Figure 3 illustrates the grid dependency test for  $\phi = 18^\circ, \alpha = 18^\circ$  and  $Ra = 10^3$ , where the most suitable mesh was deduced to be the 15828 cells density.

$$\left| \frac{Nu_i - Nu_{i-1}}{Nu_i} \right| \leq 0.01 \tag{8}$$

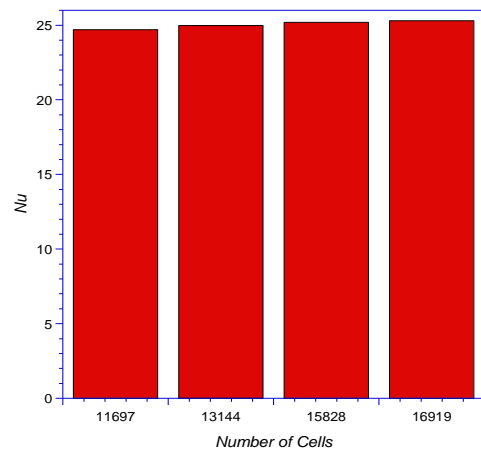


Fig. 3: Grid dependence graph

This current study is validated and compared with Koca et al. (2007). figure 4 shows the graph of  $Nu$  against  $Ra$ . Their results show a similar pattern and error deviation of 17%.

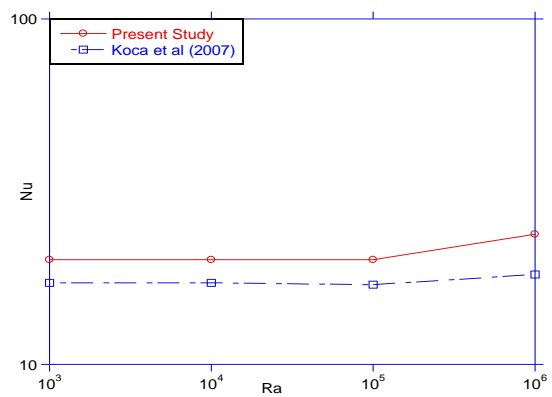


Fig. 4: Comparison of the present study with Koca et al (2007)

### 4 RESULTS AND DISCUSSION

The results of the heat transfer analysis in terms of the influence of pitch angles (top & base) and  $Ra$  on  $Nu$  and entropy generation rate are presented here. Figures 5 - 6 show that for fixed  $Ra = 10^3$  while  $\alpha = 14^\circ - 22^\circ$  and  $\phi = 14^\circ - 22^\circ$ . It is observed that  $Nu$  increases as  $\alpha$  decreases while  $Nu$  slightly increases as  $\phi$  increases. The physical implication of this is that, for a Saltbox roof type geometry, at fixed  $Ra$ , the best convective heat transfer process is achieved by lowering  $\alpha$  and increasing  $\phi$ , thus improving the thermal comfort in the building.

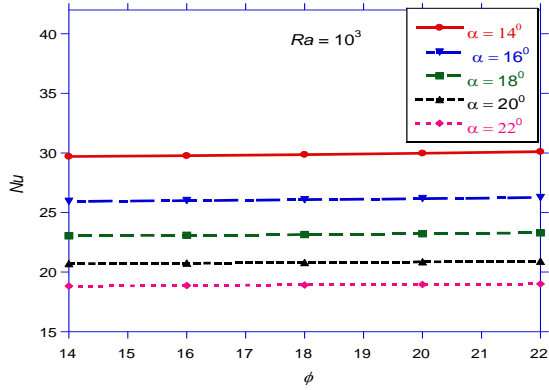


Fig. 5:  $\phi$  vs.  $Nu$  for fixed  $Ra=10^3$  at different  $\alpha$

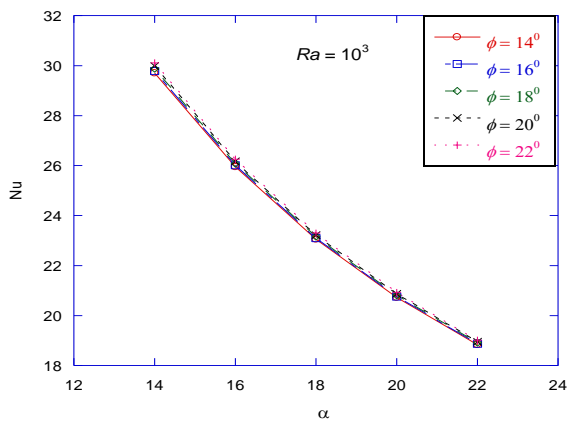


Fig. 6:  $\alpha$  against  $Nu$  for different  $\phi$  at fixed  $Ra=10^3$ .

Figures 7 - 8 show the effect of  $Ra$  on  $Nu$  at fixed  $\alpha$  and  $\phi$ . It is observed that  $Nu$  increases as  $\alpha$  decreases and  $\phi$  increases.  $Nu$  is fairly constant at low  $Ra$  and sharply increases at  $Ra > 10^5$  when  $\alpha$  is fixed and slightly increases at  $Ra > 10^6$  when  $\phi$  is fixed.

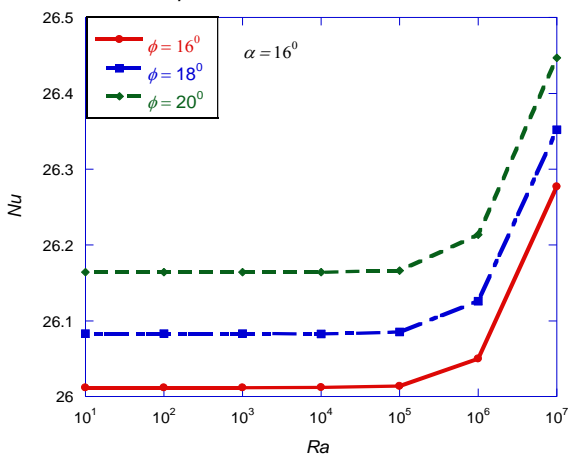


Fig. 7:  $Ra$  against  $Nu$  at different  $\phi$  and fixed  $\alpha = 16^\circ$

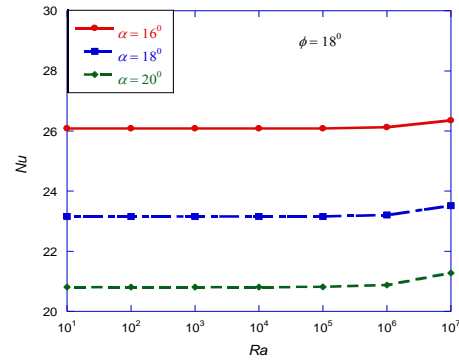


Fig. 8:  $Ra$  against  $Nu$  at different  $\alpha$  and fixed  $\phi = 18^\circ$

This indicates that at the lower  $Ra \leq 10^5$ , the heat transfer effect is controlled by conduction. Then at  $Ra > 10^5$ , the  $Nu$  is seen to have an increase, indicating the onset of convection mechanism on the heat transfer effect in the roofing geometry, as a result of stronger circulation at this stage. It implies thermal comfort would be improved at higher  $Ra$ . Figures 9 - 10 show the effect of  $\alpha$  on the various entropy generation at fixed  $Ra = 10^5$  and different  $\phi$ . It is observed that increasing  $\alpha$  causes an increase in  $S_{friction}$ , and a decrease in  $S_{thermal}$  and  $S_{Total}$ . Since energy losses in a system cause entropy generation, it implies that the energy losses in the saltbox roof type can be minimized by increasing  $\alpha$ .

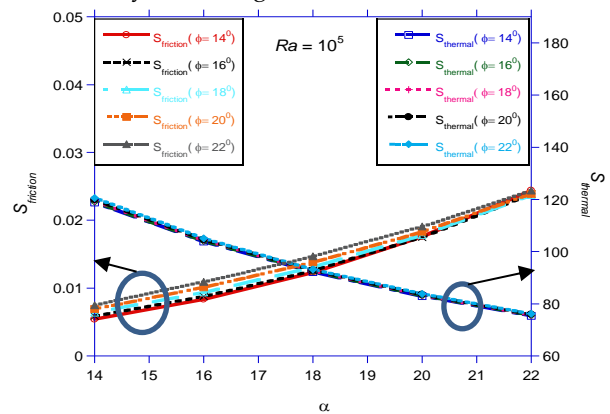


Fig. 9:  $\alpha$  against  $S_{thermal}$  and  $S_{friction}$  for different  $\phi$  and fixed  $Ra=10^5$

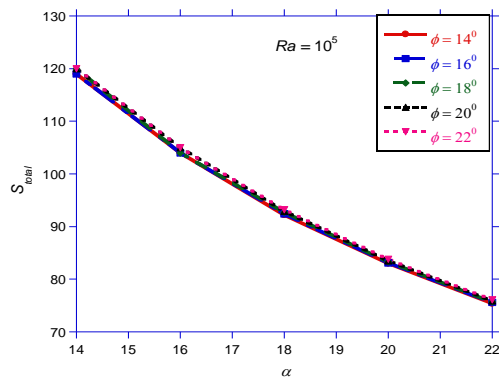


Fig. 10:  $\alpha$  against  $S_{Total}$  for different  $\phi$  at fixed  $Ra=10^5$

Figures 11 - 13 reveal the effect of  $Ra$  on  $S_{thermal}$ ,  $S_{friction}$  and  $S_{Total}$  at fixed  $\phi = 18^\circ$  and different  $\alpha$ . It is observed that as  $Ra$  increases,  $S_{thermal}$  and  $S_{Total}$  remain fairly

constant until  $Ra = 10^5$ , after which the effect of  $Ra$  on  $S_{thermal}$  and  $S_{Total}$  significantly increases. It is also noticed that the effect of  $Ra$  on  $S_{friction}$  is insignificant before  $Ra = 10^4$ , after which its effect becomes significant and  $S_{friction}$  increases. Also,  $S_{thermal}$  and  $S_{Total}$  decrease while  $S_{friction}$  increases as  $\alpha$  increases.

It is seen that increasing  $Ra$  causes  $S_{Total}$  to rise. This is due to increased heat transfer losses as the  $Ra$  rises, which affects the Entropy generation by causing an increase in irreversibility. This agrees with Hussein et al. (2016).

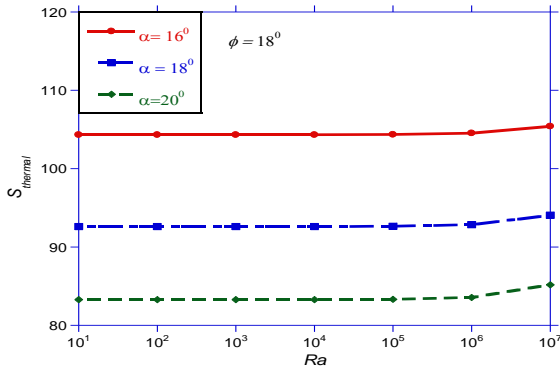


Fig. 11: Ra against  $S_{thermal}$  at fixed  $\phi = 18^\circ$  and different  $\alpha$

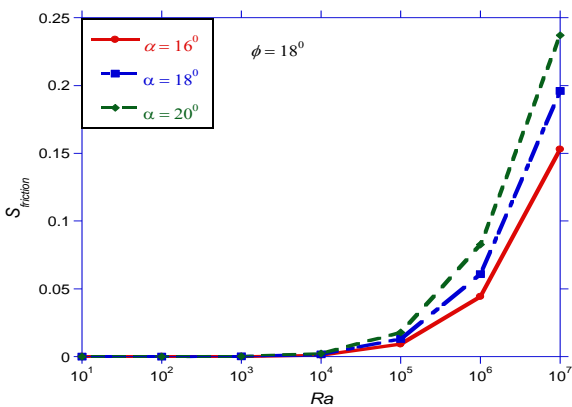


Fig. 12: Ra against  $S_{friction}$  at fixed  $\phi = 18^\circ$  and different  $\alpha$

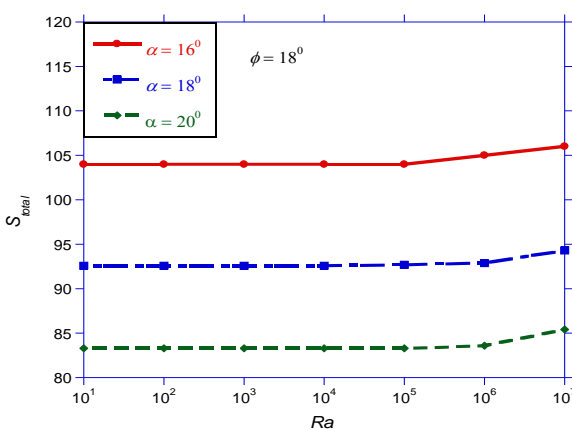


Fig. 13: Ra against  $S_{Total}$  at fixed  $\phi = 18^\circ$  and different  $\alpha$

Figure 14 shows the isotherms and streamlines at  $Ra = 10^3$ - $10^7$ . It is observed that at lower  $Ra = 10^3$  and  $10^5$ , the circulation inside the geometry is weak and unsteady, and hence the buoyant forces are weak at this stage.

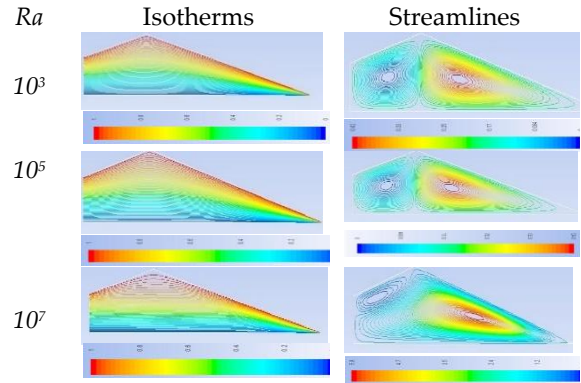


Fig. 14: Isotherms and Streamlines at different Rayleigh numbers for Saltbox

For a higher  $Ra = 10^7$ , the buoyant forces become more effective as the circulation is seen to intensify more, implying a better convective heat transfer process. In addition, it is observed from the streamline; that at lower  $Ra$ , the flow is nearly symmetric, with two counter-rotating cells dominating the flow. However, at a higher  $Ra$ , the flow becomes asymmetric and it can be seen that a strong primary cell dominates the flow in this case.

### 8 CONCLUSION

A numerical study has been carried out for the 2D laminar natural convection in saltbox roof type under summer climate conditions to study the effect of pitch angles (top and base) and  $Ra$  on heat transfer and entropy generation. It is observed that for fixed  $Ra$ ,  $Nu$  increases as  $\alpha$  decreases while  $Nu$  remains fairly constant as  $\phi$  increases. Also at fixed  $Ra$ ,  $S_{thermal}$  and  $S_{Total}$  increase while  $S_{friction}$  reduces as  $\alpha$  decreases and  $\phi$  increases. The increase in  $S_{Total}$  is due to thermal irreversibility.

However, the effect of  $Ra$  on  $Nu$  is not significant until  $Ra > 10^5$  and  $Ra > 10^6$  for fixed  $\alpha$  and  $\phi$  respectively. Also, at  $Ra = 10^1$ - $10^5$ , the heat transfer effect is controlled by conduction. At  $Ra > 10^5$ , the  $Nu$  increases, indicating the onset of convection mechanism on the heat transfer effect in the roofing geometry, resulting in stronger circulation. From streamlines and isotherms, at  $Ra \leq 10^5$ , the flow field is seen to be nearly symmetric, while flow becomes asymmetric at  $Ra > 10^5$ . It implies thermal comfort is improved at higher  $Ra$ . At fixed  $Ra$ , the best convective heat transfer process is achieved by lowering  $\alpha$  and increasing  $\phi$ .

### REFERENCES

Akinsete, V. A., & Coleman, T. A. (1982). Heat Transfer by Steady Laminar Free Convection in Triangular Enclosures. *International Journal of Heat and Mass Transfer*, 25(7), 991-998.

Alnaqi, A. A., Hussein, A. K., Kolsi, L., Al-Rashed, A. A., Li, D., & Ali, H. M. (2020). Computational Study of Natural Convection and Entropy Generation in 3-D Cavity with Active Lateral Walls. *Thermal Science*, 24(3), 2089-2100. Doi: 10.2298/TSCI180810346A

Bondareva, N.S., Sheremet, M.A., Oztop, H.F., & Abu-Hamdeh, N. (2017). Entropy Generation Due to Natural Convection of a Nanofluid in a Partially Open Triangular Cavity. *Advanced Powder Technology*, 28 (1), 244-255. DOI: 10.1016/j.apt.2016.09.030

Hussein, A.K., Lioua, K., Chand, R., Sivasankaran, S., Nikbakhti, R., Li, D., Naceur, B.M., & Habib, B.A. (2016). Three-Dimensional

- Unsteady Natural Convection and Entropy Generation in an Inclined Cubical Trapezoidal Cavity with an Isothermal Bottom Wall. *Alexandria Engineering Journal*, 55(2), 741-755.  
<https://doi.org/10.1016/j.aej.2016.01.004>
- Ishak, M. S., Alsabery, A. L., Hashim, I., & Chamkha, A. J. (2021). Production and Mixed Convection Within Trapezoidal Cavity having Nanofluids and Localised Solid Cylinder. *Scientific reports*, 11(1), 1-22. <https://doi.org/10.1038/s41598-021-94238-w>
- Koca, A., Oztop, H.F., Varol, Y. (2007). Effects of Geometrical Shape of Roofs on Natural Convection for Winter Conditions. *Proceedings of Clima Wellbeing Indoors*.
- Oztop, H. F., Kolsi, L., Alghamdi, A., Abu-Hamdeh, N., Borjini, M. N., & Aissia, H. B. (2017). Numerical Analysis of Entropy Generation due to Natural Convection in Three-Dimensional Partially Open Enclosures. *Journal of the Taiwan Institute of Chemical Engineers*, 75, 131-140.  
<https://doi.org/10.1016/j.jtice.2017.03.014>
- Patankar, S. V., & Spalding, D. B. (1972). A Calculation Procedure for Heat, Mass and Momentum Transfer in Three Dimensional Parabolic Flows. *International Journal of Heat and Mass Transfer*, 15, 1787-1806.
- Solomon, E., Kamiyo, O. (2020). Natural Convection and Flow Simulation in Right-Angled Triangular Rooftop Enclosure under Winter Condition. *International Organization of Scientific Research*, 17 (2), 07-15. doi:10.9790/1684-1702040715
- Varol, Y., Koca, A., & Oztop, H.F. (2006). Laminar Natural Convection in Saltbox Roofs for both Summerlike and Winterlike Boundary Conditions. *Journal of Applied Sciences*, 6(12), 2617-2622. <http://dx.doi.org/10.3923/jas.2006.2617.2622>
- Yang, X., Shao, Q., Hoteit, H., Carrera, J., Younes, A., & Fahs, M. (2021). Three-Dimensional Natural Convection, Entropy Generation and Mixing in Heterogeneous Porous Medium. *Advances in Water Resources*, 155, 103992.  
<https://doi.org/10.1016/j.advwatres.2021.103992>
- Zhang, X. H., Saeed, T., Algehyne, E. A., El Shorbagy, M. A., El-Refaey, A. M., & Ibrahim, M. (2021). Effect of L-Shaped Heat Source and Magnetic Field on Heat Transfer and Irreversibilities in Nanofluid-Filled Oblique Complex Enclosure. *Scientific Reports*, 11(1), 1-19. <https://doi.org/10.1038/s41598-021-95803-z>